PHYSICAL REVIEW B **95**, 201110(R) (2017)

Time-reversal and rotation symmetry breaking superconductivity in Dirac materials

Luca Chirolli,[1,*] Fernando de Juan,[1,2] and Francisco Guinea[1,3]
[1]*IMDEA-Nanoscience, Calle de Faraday 9, E-28049 Madrid, Spain*
[2]*Rudolf Peierls Centre for Theoretical Physics, 1 Keble Road, Oxford OX1 3NP, United Kingdom*
[3]*Department of Physics and Astronomy, University of Manchester, Oxford Road, Manchester M13 9PL, United Kingdom*
(Received 18 November 2016; revised manuscript received 17 February 2017; published 22 May 2017)

We consider mixed symmetry superconducting phases in Dirac materials in the odd-parity channel, where pseudoscalar and vector order parameters can coexist due to their similar critical temperatures when attractive interactions are of a finite range. We show that the coupling of these order parameters to unordered magnetic dopants favors the condensation of time-reversal symmetry breaking (TRSB) phases, characterized by a condensate magnetization, rotation symmetry breaking, and simultaneous ordering of the dopant moments. We find a rich phase diagram of mixed TRSB phases characterized by peculiar bulk quasiparticles, with Weyl nodes and nodal lines, and distinctive surface states. These findings are consistent with recent experiments on $Nb_xBi_2Se_3$ that report evidence of point nodes, nematicity, and TRSB superconductivity induced by Nb magnetic moments.

DOI: 10.1103/PhysRevB.95.201110

Introduction. One of the most fascinating aspects of unconventional superconductivity is that the condensate can display spontaneous time-reversal symmetry breaking (TRSB), hosting an intrinsic Cooper pair magnetization [1,2]. This can occur only with a multicomponent order parameter when the different components develop relative phases, as in the well-known $p+ip$ chiral state proposed for Sr_2RuO_4 or the $d+id$ state conjectured for some cuprate superconductors [1]. Experimental evidence of TRSB superconductivity has been obtained from muon spin rotation (μSR) in UPt_3 [3] and Sr_2RuO_4 [4], from the polar Kerr effect [5], and from Josephson tunneling experiments. The two-dimensional $p+ip$ state in particular has attracted great interest as a topological superconductor with protected edge and vortex modes, of potential use in the field of quantum computation [6,7]. In three dimensions, chiral superconductivity (SC) is also possible, allowing the realization of a Weyl superconductor with Majorana arcs on the surface [8–10], but realistic candidate materials for this superconducting state are lacking.

Recently, very compelling evidence for unconventional superconductivity has been reported in Dirac materials of the Bi_2Se_3 family upon doping [7,11,12]. These studies were originally motivated by the prediction of a three-dimensional, time-reversal invariant (TRI) topological superconductor featuring protected Andreev surface states [13]. However, the rich phenomenology gathered so far suggests a more complicated pairing scenario. Superconductivity was first observed in $Cu_xBi_2Se_3$ [14–16], but evidence for the characteristic surface Andreev states has remained controversial [17–19]. Moreover, nuclear magnetic resonance experiments [20] reveal that there is spin rotation symmetry breaking in the superconducting state, which rather supports a different pairing state of a nematic type [21,22]. Superconductivity was also reported in $Sr_xBi_2Se_3$ [23,24] and in $Tl_xBi_2Te_3$ [25], but evidence for unconventional pairing is lacking. Most interestingly, superconductivity has also been reported in $Nb_xBi_2Se_3$ [26], where initially paramagnetic samples were shown to develop a spontaneous magnetization at the superconducting transition. The magnetization survived only at the surface in the Meissner state, and it was claimed to originate from Nb magnetic moments. In the same compound, a later torque magnetometry experiment [27] showed clear signatures of rotation symmetry breaking, and penetration depth measurements revealed a power law dependence with temperature [28] which points to the existence of nodes in the gap.

This complicated phenomenology is perhaps best understood within the minimal model of a superconducting Dirac Hamiltonian with approximate rotation symmetry, where there are only three possible pairing channels: a conventional s-wave scalar, an odd-parity pseudoscalar, and a vector. The pseudoscalar order parameter χ corresponds to the TRI topological superconductor, while rotation symmetry breaking can only be produced by the vector $\boldsymbol{\psi}$. The condensation of $\boldsymbol{\psi}$ is therefore a prerequisite to explain current experiments, but it has previously been shown that with only local interactions the χ channel always has a higher critical temperature than the $\boldsymbol{\psi}$ channel [13]. In addition, even if χ could be ignored, $\boldsymbol{\psi}$ remains time-reversal symmetric within current models [21,29]. These two problems make the explanation of the observed phenomenology a theoretical challenge.

Motivated by recent experiments, in this Rapid Communication we develop a theory of possible TRSB superconducting phases of doped Dirac Hamiltonians in the presence of magnetic impurities. We first show that when further neighbor electron-electron interactions are included, the critical temperature of $\boldsymbol{\psi}$ is raised and can become comparable to that of χ, providing a solution to the first problem. The closeness of the critical temperatures enables different mixed symmetry phases where both order parameters can condense simultaneously, similar to $s+id$ states predicted in high-T_c superconductors [30–32]. We then develop a theory for these mixed phases, showing that the coupling of magnetic impurities, which would otherwise be paramagnetic, to the magnetization of the Cooper pairs [33–36] favors the condensation of TRSB phases and the consequent ordering of the magnetic impurities. We find three mixed TRSB phases that differ in the way rotation and gauge symmetries are broken and can be distinguished by their bulk

*luca.chirolli@imdea.org

spectrum, which may be gapped or feature Weyl nodes or nodal lines, or by the existence of surface states. We find a phase that is consistent with the surface magnetization [26], rotation symmetry breaking [27], and the existence of linear nodes [28].

Superconductivity in Dirac materials. We now consider the possible superconducting instabilities of Dirac Hamiltonians. To make contact with previous work, we start with the Hamiltonian commonly employed to describe Bi_2Se_3 [13],

$$\mathcal{H}_0 = m\sigma_x + v\sigma_z(k_x s_y - k_y s_x) + v_z k_z \sigma_y, \tag{1}$$

where s_i are spin Pauli matrices and σ_i are Pauli matrices for p_z orbitals in the top and bottom layer of the quintuple layer (QL) Bi_2Se_3 structure, v is the Fermi velocity, and m the insulating mass. The time-reversal operator is $\mathcal{T} = is_y K$, with K the complex conjugation. When $v_z = v$, this Hamiltonian is a particular realization of the isotropic Dirac Hamiltonian of the form

$$\mathcal{H}_0 = \gamma_0 m + v\gamma_0\gamma_i k_i, \tag{2}$$

where the Euclidean gamma matrices $\gamma_\mu = (\gamma_0, \gamma_i)$ satisfy $[\gamma_\mu, \gamma_\nu]_+ = \mathcal{I}_{\mu\nu}$ and are given by $\gamma_\mu = (\sigma_x, -\sigma_y s_y, \sigma_y s_x, \sigma_z)$. Here, we will preferentially use the general Dirac matrices to emphasize the structure of the rotation group: γ_i transforms as a vector, γ_0 as a scalar, and the matrix $\gamma_5 \equiv \gamma_0\gamma_1\gamma_2\gamma_3$ as a pseudoscalar.

To classify the possible pairing channels, we introduce the Nambu spinor $\Psi_{\mathbf{k}} = (\mathbf{c}^\dagger_{\mathbf{k}}, is_y\mathbf{c}_{-\mathbf{k}})^T$, with $\mathbf{c}_{\mathbf{k}}$ fermionic annihilation operators of $\mathcal{H}_0$, and consider the Bogoliubov–de Gennes Hamiltonian $\hat{H} = \frac{1}{2}\int d\mathbf{k}\Psi^\dagger_{\mathbf{k}}\mathcal{H}_{\mathbf{k}}\Psi_{\mathbf{k}}$, with

$$\mathcal{H}_{\mathbf{k}} = [\mathcal{H}_0(\mathbf{k}) - \mu]\tau_z + \Delta_{\mathbf{k}}\tau_+ + \Delta^\dagger_{\mathbf{k}}\tau_-, \tag{3}$$

where μ is the chemical potential, $\Delta_{\mathbf{k}}$ stands for generic momentum-dependent 4×4 pairing matrices, and τ_i Pauli matrices act in the particle-hole space. The Nambu construction imposes the charge conjugation symmetry $\mathcal{C}$ implemented as $U_{\mathcal{C}}\mathcal{H}(-\mathbf{k})^* U^\dagger_{\mathcal{C}} = -\mathcal{H}(\mathbf{k})$, with $U_{\mathcal{C}} = s_y\tau_y$, which amounts to the restriction $s_y\Delta^*(-\mathbf{k})s_y = \Delta(\mathbf{k})$. If pairing is momentum independent [13,37], only six possible matrices in the Dirac algebra satisfy this constraint: the two even-parity scalars I and γ^0, and the pseudoscalar γ^5 and the vector γ^i, which are both odd under parity. Disregarding the even-parity scalars, the pairing matrix takes the form $\Delta = \chi\gamma^5 + \boldsymbol{\psi}\cdot\boldsymbol{\gamma}$. For the specific model of Bi_2Se_3, it was concluded that the local interorbital interaction V can give rise to pairing in both of these channels, but the critical temperatures of the two channels satisfy $T_\chi \gg T_\psi$ [13], which makes it unlikely for the system to condense in the vector channel as stated previously.

We suggest that this problem can be solved by considering momentum-dependent corrections to the two-body interorbital density-density interaction. At lowest order in $\mathbf{q} = \mathbf{k} - \mathbf{k}'$, one has

$$V(\mathbf{k},\mathbf{k}') = V(1 + a^2\mathbf{k}\cdot\mathbf{k}'), \tag{4}$$

with a a length scale on order of the lattice constant. In order to decouple the additional momentum-dependent interaction term we need to consider the other ten matrices in the Dirac algebra [38]. In particular, we note that that pairing matrix $\gamma^5\gamma^i k^j\epsilon_{ijk}$ is also a vector, and it modifies the gap matrix as

$$\Delta_{\mathbf{k}} = \chi\gamma^5 + \boldsymbol{\psi}\cdot(\boldsymbol{\gamma} - ia\gamma^5\boldsymbol{\gamma}\times\mathbf{k}). \tag{5}$$

It is instructive to project the 4×4 Dirac matrices into the 2×2 space of the Kramers degenerate conduction band states relevant to pairing [29]. If we define Pauli matrices $\tilde{s}_i$ for this space, the gap matrix takes the form $\Delta_{\mathbf{k}} = \chi\tilde{\mathbf{k}}\cdot\tilde{\mathbf{s}} + \boldsymbol{\psi}\times\tilde{\mathbf{k}}\cdot\tilde{\mathbf{s}}(1 + \mu a/v)$, with $\tilde{\mathbf{k}} = v\mathbf{k}/\mu$. Thus, while seemingly of higher order in the Dirac Hamiltonian, the correction term is actually of the same order when projected to the Fermi surface. The momentum dependence of the pairing interaction affects only the vector channel and it raises its critical temperature T_ψ, which becomes comparable to T_χ [38].

Ginzburg-Landau free energy. We now consider superconductivity at the level of the Ginzburg-Landau (GL) free energy. The pseudoscalar order parameter free energy is

$$F_\chi = a_1|\chi|^2 + b_1|\chi|^4 \tag{6}$$

and condensation of χ takes place when $a_1(T_\chi) = 0$. For the vector order parameter $\boldsymbol{\psi}$, symmetry dictates that the form of the free energy be [39,40]

$$F_\psi = a_2|\boldsymbol{\psi}|^2 + b_2|\boldsymbol{\psi}|^4 + b_2'|\boldsymbol{\psi}\times\boldsymbol{\psi}^*|^2. \tag{7}$$

The vector representation admits two possible superconducting states: a nematic state $\boldsymbol{\psi}\propto(1,0,0)$ which is time-reversal invariant, and a chiral TRSB state $\boldsymbol{\psi}\propto(1,\pm i,0)$ [21,29]. The sign of the coupling b_2' determines whether the vector representation chooses the nematic (for $b_2' > 0$) or the chiral state (for $b_2' < 0$). Since at second order no coupling is allowed by symmetry between χ and $\boldsymbol{\psi}$, the condensation of $\boldsymbol{\psi}$ takes place when $a_2(T_\psi) = 0$. However, our previous argument suggesting that $a_1 \sim a_2$ [38] and $T_\chi \sim T_\psi$ requires that we study a coupled theory beyond second order where both order parameters may coexist. At fourth order the coupling term in the GL free energy reads

$$F_{\psi,\chi} = d_1|\chi|^2|\boldsymbol{\psi}|^2 + d_2|\chi^*\boldsymbol{\psi} - \chi\boldsymbol{\psi}^*|^2, \tag{8}$$

and the total free energy is

$$F = F_\chi + F_\psi + F_{\chi,\psi}. \tag{9}$$

In the weak coupling regime with $a_1 \sim a_2$ both order parameters acquire a finite value.

The possible TRSB phases arising from this free energy are characterized by a magnetization of the condensate, due to the spin triplet state of the Cooper pairs. By symmetry, the magnetization must be built with gauge invariant combinations of order parameters and transform as a spin, i.e., as a $\mathcal{T}$-odd pseudovector (even under inversion). Since $\boldsymbol{\psi}$ is a vector and χ a pseudoscalar, the following combinations satisfy the symmetry requirements,

$$\boldsymbol{\Sigma}_1 = \chi\boldsymbol{\psi}^* - \chi^*\boldsymbol{\psi}, \quad \boldsymbol{\Sigma}_2 = \boldsymbol{\psi}\times\boldsymbol{\psi}^*.$$

Note that $\boldsymbol{\Sigma}_1$ cannot be built with a standard s-wave order parameter because the combination would not be a pseudovector. These two pseudovectors are orthogonal and appear quadratically in the GL Eqs. (7) and (8).

The different possible phases obtained from the GL free energy Eq. (9) are realized with different signs of the interaction

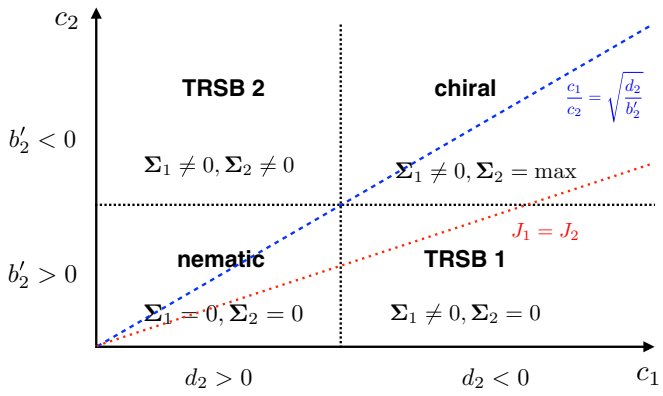

FIG. 1. Phase diagram of superconductivity involving the pseudoscalar and the vector order parameters coupled to the dopants' magnetization. The four possible phases can be obtained by properly tuning the couplings J_1 and J_2.

parameters b_2' and d_2 and can be distinguished by the values of $\mathbf{\Sigma}_1$ and $\mathbf{\Sigma}_2$ and the way rotation and gauge symmetries are broken. For $d_2, b_2' > 0$, one has $\mathbf{\Sigma}_1 = \mathbf{\Sigma}_2 = \mathbf{0}$ and the system is in the TRI nematic phase, with rotation symmetry about the nematic director. When $d_2 < 0$ and $b_2' > 0$, one has $\mathbf{\Sigma}_1 \neq \mathbf{0}$ and $\mathbf{\Sigma}_2 = \mathbf{0}$, and the system is invariant under rotations about $\mathbf{\Sigma}_1$. We name this phase TRSB 1. When $d_2, b_2' < 0$, one has $\mathbf{\Sigma}_2 \neq \mathbf{0}$, and the system is in the chiral phase, with $\boldsymbol{\psi} \propto (1, i, 0)$. In this case the system is invariant under rotations around $\mathbf{\Sigma}_2$ combined with a gauge transformation [38]. Finally, when $d_2 > 0$ and $b_2' < 0$, one has $\mathbf{\Sigma}_2 \neq \mathbf{0}$, but $\boldsymbol{\psi}$ is not in the purely chiral state, but rather in a hybrid solution [38] which has no symmetry. We name this phase TRSB 2.

A schematic phase diagram as a function of b_2' and d_2 is depicted in Fig. 1. Microscopic calculations [21,29,38] show that for an isotropic model $b_2', d_2 > 0$, precluding a TRSB phase. We show next how a coupling to magnetic dopants renormalizes the coefficients b_2' and d_2 and can change their sign if the coupling is strong enough.

Coupling to dopant magnetization. The presence of random magnetic moments in the sample can be described by an average magnetization $\mathbf{M}$. At the Landau theory level, both $\mathbf{\Sigma}_1$ and $\mathbf{\Sigma}_2$ can couple linearly to $\mathbf{M}$ [33–36], which is also a $\mathcal{T}$-odd pseudovector,

$$F_{\chi,\boldsymbol{\psi},M} = i\mathbf{M} \cdot [c_1(\chi \boldsymbol{\psi}^* - \chi^* \boldsymbol{\psi}) + c_2 \boldsymbol{\psi} \times \boldsymbol{\psi}^*]. \tag{10}$$

By appropriately aligning $\mathbf{M}$, we see that the system may lower its energy by condensing in a TRSB phase with finite condensate magnetizations.

Neglecting interactions between the magnetic moments, the full free energy at second order in $\mathbf{M}$ including the superconducting order parameters reads

$$F = a_3 |\mathbf{M}|^2 + F_\chi + F_\psi + F_{\chi,\psi} + F_{\chi,\psi,M}. \tag{11}$$

Since the dopants are paramagnetic above T_c, we assume $a_3 > 0$. The mean-field solution for $\mathbf{M}$ can be found by minimizing the free energy with respect to $\mathbf{M}$, finding $\mathbf{M} = -i\frac{c_1}{2a_3}\mathbf{\Sigma}_1 - i\frac{c_2}{2a_3}\mathbf{\Sigma}_2$. It is clear that a nonzero magnetization $\mathbf{M}$ arises in all TRSB phases, despite the fact that the dopants are initially paramagnetic. Substituting the mean-field value of the magnetization, the free energy takes the form of Eq. (9) with modified parameters

$$d_2 \to d_2 - \frac{c_1^2}{4a_3}, \quad b_2' \to b_2' - \frac{c_2^2}{4a_3}. \tag{12}$$

Since the coupling to magnetic dopants renormalizes both b_2' and d_2, with different values of c_1 and c_2 one can now span the entire phase diagram in Fig. 1.

Meissner screening. The presence of the magnetic dopants induces the condensation of a TRSB phase where the dopants' moments are aligned with the spin magnetization of the condensate. The resulting total spin magnetization $\mathbf{M}_s = \mathbf{M} + i\mu(\mathbf{\Sigma}_1 + \mathbf{\Sigma}_2)$ acts back onto the orbital degrees of freedom and the GL free energy is [41,42]

$$\mathcal{F} = \int d\mathbf{r} \left[F + \frac{\mathbf{B}^2}{8\pi} - \mathbf{B} \cdot \mathbf{M}_s + F^{\text{grad}}_{\chi,\boldsymbol{\psi},\mathbf{M}} \right], \tag{13}$$

where $\mathbf{B}$ is the full induction field and F^{grad} accounts for gradient terms for the order parameters [38]. For finite $\mathbf{M}_s$ the system may develop screening supercurrents, so that $\mathbf{B} = \mathbf{H} + 4\pi(\mathbf{M}_s + \mathbf{M}_o)$, with $\mathbf{M}_o$ the orbital magnetization due to screening currents, and $\mathbf{H}$ an external field. For $\mathbf{H} = \mathbf{0}$, the order parameters in the bulk can be taken to be constant, so that $\mathbf{B} = \mathbf{0}$ by Meissner screening, provided that $M_s < H_{cr}$, with H_{cr} the thermodynamic critical field [38,41]. Since M_s is linked to the mean-field value of χ and $\boldsymbol{\psi}$, for $a_1 \sim a_2$ the ratio M_s/H_{cr} is temperature independent and it is suppressed by strong b_1 and b_2. At the surface of the system the cancellation between spin and orbital magnetization is not satisfied locally, due to difference in the coherence length, penetration depth, and the length scale of variation of $\mathbf{M}$, and a finite surface magnetization may arise, in agreement with the observations of Ref. [26].

Microscopic coupling. The coupling Eq. (10) and the resulting phase diagram is generic of a SO(3) invariant theory. The only symmetry allowed microscopic coupling must be written in terms of the spin pseudovectors $\mathbf{S}_\parallel \equiv (s_x, s_y, \sigma_x s_z)$ and $\mathbf{S}_\perp \equiv (\sigma_x s_x, \sigma_x s_y, s_z)$ [38],

$$H_Z = J_1 \mathbf{M} \cdot \mathbf{S}_\parallel + J_2 \mathbf{M} \cdot \mathbf{S}_\perp. \tag{14}$$

The coefficients c_1 and c_2 can be derived microscopically from this coupling, and doing so reveals the constraint $c_1(J_1 m/\mu + J_2) = 2c_2(J_1 + J_2 m/\mu)$ [38]. All phases in Fig. 1 can therefore be realized by properly tuning J_1, J_2, and m/μ. In Bi_2Se_3, the SO(3) symmetry breaks down to the lattice point group D_{3d} when anisotropy corrections are included [13]. The vector $\boldsymbol{\psi} = (\psi_x, \psi_y, \psi_z)$ splits into two-component $E_u \sim (-\psi_y, \psi_x)$ and one-component $A_{2u} \sim \psi_z$ representations. The pseudoscalar χ corresponds to the A_{1u} representation. A microscopic coupling between the magnetic moments and the physical spin $\mathbf{s}$ of the electrons in Bi_2Se_3 can be written in terms of a Zeeman coupling $H_Z = -J(s_x M_x + s_y M_y) - J_z s_z M_z$, with $J \neq J_z$ the anisotropic Zeeman coupling constants. The resulting phase diagram remains qualitatively very similar to the SO(3) invariant one [38].

Gap structure. The value of the superconducting gap on the Fermi surface for the different phases depends on the relative strength of the two order parameters. When χ dominates all phases are fully gapped, but different cases arise if $\boldsymbol{\psi}$ dominates. In the nematic case the gap has Dirac nodes along

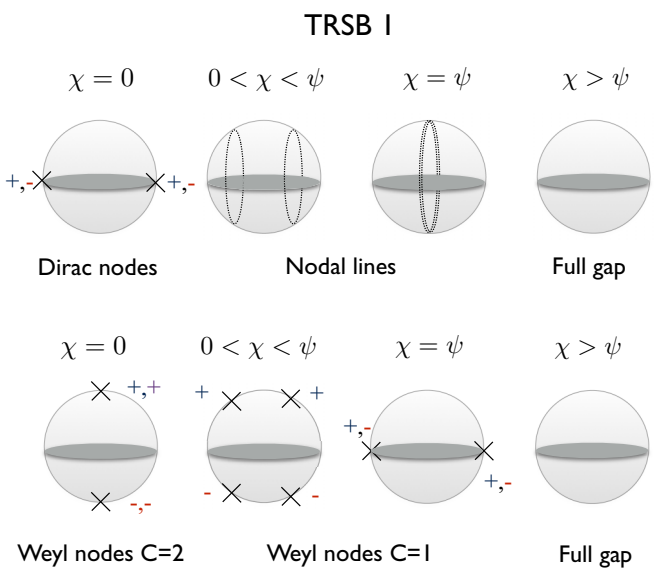

FIG. 2. Schematics of the gap structure on the Fermi surface: TRSB 1 has Dirac nodes that evolve in a nodal line for $\chi > 0$. TRSB 2 and the chiral phase have Weyl points with $C = 2$ that split in two $C = 1$ upon switching χ. The phases are fully gapped for $\chi > \psi$.

the nematic direction for $\chi = 0$. These nodes can be gapped by a small χ or by hexagonal warping terms [21], so that in general the phase is fully gapped. In the TRSB 1 phase the order parameters may be taken as $\boldsymbol{\psi} = \psi_0(1,0,0)$ and $\chi = \chi_0 e^{i\gamma}$ and that the Dirac nodes for $\chi = 0$ can be shown to become circular nodal lines defined by $\sin\theta = \pm\chi_0/\psi_0$, with θ the polar angle with respect to $\boldsymbol{\Sigma}_1$. Nodal lines of the north and south hemisphere join for $\chi = \psi$ and become gapped for $\chi > \psi$ (see Fig. 2). These nodal lines have a linear density of states (DOS) $\rho(\epsilon) \propto \epsilon$ [43]. In the chiral and the TRSB 2 phase a Weyl superconductor is realized [8–10,29]. For $\chi = 0$ there are Weyl nodes of topological charge $C = \pm 2$ on the north and south pole along the direction of $\boldsymbol{\Sigma}_2$ [44]. For finite χ these nodes are split into two Weyl nodes of $C = 1$ at a finite polar angle, and in the azimuthal direction given by Σ_1 and by increasing χ they move towards the equator where they meet with the nodes from the south hemisphere and gap out for $\chi > \psi$ (see Fig. 2). Note that while the DOS is linear in energy when $\chi = 0$, $\rho_{C=2}(\epsilon) \propto \epsilon$, it becomes quadratic for finite χ, $\rho_{C=1}(\epsilon) \propto \epsilon^2$ [45]. These predictions could be confirmed by scanning tunneling microscopy (STM) or specific heat measurements. On the surface of a Weyl superconductor there are Majorana arcs of different kinds [44], while in the gapped phases the topologically protected surface Andreev states associated with χ are gapped on the surfaces orthogonal to $\boldsymbol{\Sigma}_1$.

Discussion and conclusions. The features of the TRSB2 phase predicted in this Rapid Communication are consistent with all the observations made in recent experiments with $Nb_xBi_2Se_3$: the breaking of rotation [27] and time-reversal symmetry [26] and the presence of point nodes [28]. These conclusions remain valid also if the scalar and vector representations are split due to lattice symmetries. In this case, the lattice will naturally pin the direction of Σ_2 to the c axis, while Σ_1 will lay in plane, pointing in a high-symmetry direction. This is enough to reproduce the twofold pattern observed in torque magnetometry. Our work makes the additional prediction that the magnetization, which can only be observed in the surface due to Meissner screening, must have both in-plane and out-of-plane components. The TRSB2 phase also features linear nodes in the bulk with Chern number $C = 1$, consistent with the scaling of the penetration depth. This is in contrast with the TRI nematic candidate state, which was argued to be fully gapped in the presence of trigonal warping [21]. Our work further predicts the positions of the nodes to lie in the direction of Σ_1, a prediction that could be tested, for example, with the nodal spectroscopy techniques proposed in Refs. [46–48]. Finally, our work also provides a general framework to address current and future experiments with doped Dirac materials, emphasizing the importance of mixed symmetry states and coexistence of order parameters.

Note added. Recently, we became aware of Ref. [49], where magnetic Nb dopants are also considered as the mechanism that stabilizes chiral superconductivity. This work does not provide a mechanism for the vector channel to compete with the pseudoscalar, and no mixed symmetry phases are considered. The chiral state proposed in Ref. [49] respects C_3 rotation symmetry, in contrast with Ref. [27]. The issue of Meissner screening is also not addressed.

Acknowledgment. The authors acknowledge useful discussions with Irina Grigorieva. The authors acknowledge funding from the European Union's Seventh Framework Programme (FP7/2007-2013) through the ERC Advanced Grant NOVGRAPHENE through Grant Agreement No. 290846 (L.C., F.J., and F.G.), from the Marie Curie Programme under EC Grant Agreement No. 705968 (F.J.), and from the European Commission under the Graphene Flagship, Contract No. CNECTICT-604391 (F.G.).

[1] M. Sigrist and K. Ueda, Rev. Mod. Phys. **63**, 239 (1991).

[2] Y. Maeno, H. Hashimoto, K. Yoshida, S. Nishizaki, T. Fujita, J. G. Bednorz, and F. Lichtenberg, Nature (London) **372**, 532 (1994).

[3] G. M. Luke, A. Keren, L. P. Le, W. D. Wu, Y. J. Uemura, D. A. Bonn, L. Taillefer, and J. D. Garrett, Phys. Rev. Lett. **71**, 1466 (1993).

[4] G. M. Luke, Y. Fudamoto, K. M. Kojima, M. I. Larkin, J. Merrin, B. Nachumi, Y. J. Uemura, Y. Maeno, Z. Q. Mao, Y. Mori *et al.*, Nature **394**, 558 (1998).

[5] A. Kapitulnik, J. Xia, E. Schemm, and A. Palevski, New J. Phys. **11**, 055060 (2009).

[6] C. Nayak, S. H. Simon, A. Stern, M. Freedman, and S. Das Sarma, Rev. Mod. Phys. **80**, 1083 (2008).

[7] X.-L. Qi and S.-C. Zhang, Rev. Mod. Phys. **83**, 1057 (2011).

[8] T. Meng and L. Balents, Phys. Rev. B **86**, 054504 (2012).
[9] J. D. Sau and S. Tewari, Phys. Rev. B **86**, 104509 (2012).
[10] S. A. Yang, H. Pan, and F. Zhang, Phys. Rev. Lett. **113**, 046401 (2014).
[11] H. Zhang, C.-X. Liu, X.-L. Qi, X. Dai, Z. Fang, and S.-C. Zhang, Nat. Phys. **5**, 438 (2009).
[12] M. Z. Hasan and C. L. Kane, Rev. Mod. Phys. **82**, 3045 (2010).
[13] L. Fu and E. Berg, Phys. Rev. Lett. **105**, 097001 (2010).
[14] Y. S. Hor, A. J. Williams, J. G. Checkelsky, P. Roushan, J. Seo, Q. Xu, H. W. Zandbergen, A. Yazdani, N. P. Ong, and R. J. Cava, Phys. Rev. Lett. **104**, 057001 (2010).
[15] L. A. Wray, S.-Y. Xu, Y. Xia, Y. S. Hor, D. Qian, A. V. Fedorov, H. Lin, A. Bansil, R. J. Cava, and M. Z. Hasan, Nat. Phys. **6**, 855 (2010).
[16] M. Kriener, K. Segawa, Z. Ren, S. Sasaki, and Y. Ando, Phys. Rev. Lett. **106**, 127004 (2011).
[17] S. Sasaki, M. Kriener, K. Segawa, K. Yada, Y. Tanaka, M. Sato, and Y. Ando, Phys. Rev. Lett. **107**, 217001 (2011).
[18] N. Levy, T. Zhang, J. Ha, F. Sharifi, A. A. Talin, Y. Kuk, and J. A. Stroscio, Phys. Rev. Lett. **110**, 117001 (2013).
[19] H. Peng, D. De, B. Lv, F. Wei, and C. W. Chu, Phys. Rev. B **88**, 024515 (2013).
[20] K. Matano, M. Kriener, K. Segawa, Y. Ando, and G.-q. Zheng, Nat. Phys. **12**, 852 (2016).
[21] L. Fu, Phys. Rev. B **90**, 100509(R) (2014).
[22] J. W. F. Venderbos, V. Kozii, and L. Fu, Phys. Rev. B **94**, 094522 (2016).
[23] Shruti, V. K. Maurya, P. Neha, P. Srivastava, and S. Patnaik, Phys. Rev. B **92**, 020506 (2015).
[24] Z. Liu, X. Yao, J. Shao, M. Zuo, L. Pi, S. Tan, C. Zhang, and Y. Zhang, J. Am. Chem. Soc. **137**, 10512 (2015).
[25] Z. Wang, A. A. Taskin, T. Frölich, M. Braden, and Y. Ando, Chem. Mater. **28**, 779 (2016).
[26] Y. Qiu, K. Nocona Sanders, J. Dai, J. E. Medvedeva, W. Wu, P. Ghaemi, T. Vojta, and Y. San Hor, arXiv:1512.03519.
[27] T. Asaba, B. J. Lawson, C. Tinsman, L. Chen, P. Corbae, G. Li, Y. Qiu, Y. S. Hor, L. Fu, and L. Li, Phys. Rev. X **7**, 011009 (2017).
[28] M. P. Smylie, H. Claus, U. Welp, W.-K. Kwok, Y. Qiu, Y. S. Hor, and A. Snezhko, Phys. Rev. B **94**, 180510(R) (2016).
[29] J. W. F. Venderbos, V. Kozii, and L. Fu, Phys. Rev. B **94**, 180504(R) (2016).
[30] G. Kotliar, Phys. Rev. B **37**, 3664 (1988).
[31] K. A. Musaelian, J. Betouras, A. V. Chubukov, and R. Joynt, Phys. Rev. B **53**, 3598 (1996).
[32] W.-C. Lee, S.-C. Zhang, and C. Wu, Phys. Rev. Lett. **102**, 217002 (2009).
[33] M. B. Walker and K. V. Samokhin, Phys. Rev. Lett. **88**, 207001 (2002).
[34] V. P. Mineev, Phys. Rev. B **66**, 134504 (2002).
[35] K. V. Samokhin and M. B. Walker, Phys. Rev. B **66**, 174501 (2002).
[36] V. P. Mineev, Int. J. Mod. Phys. B **18**, 2963 (2004).
[37] T. Hashimoto, S. Kobayashi, Y. Tanaka, and M. Sato, Phys. Rev. B **94**, 014510 (2016).
[38] See Supplemental Material at http://link.aps.org/supplemental/10.1103/PhysRevB.95.201110 for details on the Dirac matrices, the microscopic theory for Bi_2Se_3, the minimization of Landau free energies, and the gap structure on the Fermi surface.
[39] K. Ueda and T. M. Rice, Phys. Rev. B **31**, 7114 (1985).
[40] A. Knigavko and B. Rosenstein, Phys. Rev. Lett. **82**, 1261 (1999).
[41] V. L. Ginzburg, JETP **4**, 153 (1957).
[42] D. V. Shopova and D. I. Uzunov, Phys. Rev. B **72**, 024531 (2005).
[43] M. Phillips and V. Aji, Phys. Rev. B **90**, 115111 (2014).
[44] V. Kozii, J. W. F. Venderbos, and L. Fu, Sci. Adv. **2**, e1601835 (2016).
[45] C. Fang, M. J. Gilbert, X. Dai, and B. A. Bernevig, Phys. Rev. Lett. **108**, 266802 (2012).
[46] B. P. Stojkovic and O. T. Valls, Phys. Rev. B **51**, 6049 (1995).
[47] I. Zutic and O. T. Valls, Phys. Rev. B **56**, 11279 (1997).
[48] K. Halterman and O. T. Valls, Phys. Rev. B **62**, 5904 (2000).
[49] N. F. Q. Yuan, W.-Y. He, and K. T. Law, Phys. Rev. B **95**, 201109 (2017).